Journal of Applied Physics

RESEARCH ARTICLE | FEBRUARY 25 2022

Influence of strain and dislocations on GaSb/GaAs quantum dots: From nested to staggered band alignment FREE

B. C. McGuigan; A. S. Chang ; C. Greenhill ; H. T. Johnson; R. S. Goldman

Journal of Applied Physics 131, 085703 (2022)
https://doi.org/10.1063/5.0070657

Journal of Applied Physics ARTICLE scitation.org/journal/jap

Influence of strain and dislocations on GaSb/GaAs quantum dots: From nested to staggered band alignment

Cite as: J. Appl. Phys. **131**, 085703 (2022); doi: 10.1063/5.0070657
Submitted: 8 September 2021 · Accepted: 23 January 2022 ·
Published Online: 25 February 2022

View Online Export Citation CrossMark

B. C. McGuigan,[1] A. S. Chang,[2,a)] C. Greenhill,[2] H. T. Johnson,[1] and R. S. Goldman[2,b)]

AFFILIATIONS

[1]Department of Materials Science and Engineering, University of Urbana-Champaign, Urbana, Illinois 61801, USA
[2]Department of Materials Science and Engineering, University of Michigan, Ann Arbor, Michigan 48109, USA

[a)]**Present address:** Department of Materials Science and Engineering, Northwestern University, Evanston, Illinois 60208, USA.
[b)]**Author to whom correspondence should be addressed:** rsgold@umich.edu

ABSTRACT

We investigate the influence of strain and dislocations on band alignment in GaSb/GaAs quantum dot systems. Composition profiles from cross-sectional scanning tunneling microscopy images are interpolated onto a finite element mesh in order to calculate the distribution of local elastic strain, which is converted to a spatially varying band alignment using deformation potential theory. Our calculations predict that dislocation-induced strain relaxation and charging lead to significant local variations in band alignment. Furthermore, misfit strain induces a transition from a nested (type I) to a staggered (type II) band alignment. Although dislocation-induced strain relaxation prevents the type I to type II transition, electrostatic charging at dislocations induces the staggered band alignment once again.

INTRODUCTION

A nested (type I) band alignment, which facilitates electron–hole recombination, is useful for light-emitting devices. On the other hand, a staggered (type II) band alignment enables spatial separation of charge carriers, which is useful for charge-based memory[1,2] and solar cell devices.[3–5] GaAsSb based quantum structures are predicted to undergo strain and/or composition-induced transitions from type I to type II offsets.[6–8] However, there are conflicting reports in the literature regarding the experimental signature for the type I to type II transition,[9–17] and a predictive framework for the composition and strain dependence of the band offsets has yet to be developed. Conventional model solid theory,[18] which relates the average atomic electrostatic potential to the vacuum level, predicts a type I band alignment for unstrained GaSb/GaAs heterostructures (7% misfit). It has been suggested that the Sb/Ga beam-equivalent pressure (BEP) and/or the GaAs surface termination can be used to selectively nucleate coherently strained vs relaxed QDs.[19] Furthermore, for capped QDs, atomic structures ranging from QDs to QD rings to clusters have been observed.[8,14,15,20,21] Recently, a combined computational–experimental approach was used to associate increasing photoluminescence (PL) emission energies with nanostructure morphologies ranging from QDs to QD rings to 2D layers.[8] In addition, Schrödinger–Poisson simulations revealed type II band offsets for fully-strained GaSb/GaAs QDs and QD rings, with a partial-strain-relaxation-induced transition from a type II to a type I band offset for planar GaSb/GaAs heterostructures.[7,8] However, the influence of partial-strain relaxation and dislocation charging on the band offsets at non-planar GaSb-based heterostructures has not yet been reported.

In this work, we use a combined computational–experimental approach to examine the relative influences of misfit strain, dislocation strain, and dislocation charging on band alignment at the interfaces surrounding GaSb QDs buried in GaAs. For this purpose, we utilize XSTM images of buried GaSb/GaAs QDs from both Ref. 21 [Fig. 1(a)] and those from our studies. These XSTM images were selected because they contain QDs with sizes and shapes similar to those typically reported in the literature. Local elastic strain in the vicinity of a GaSb/GaAs QD is modeled using morphology and composition profiles as input into a continuum finite element model. This approach allows us to predict the influence of compositional variations on band offsets in the vicinity of GaSb/GaAs QDs. We assume the presence of misfit dislocations at the top and bottom interfaces of the QD structure, as expected for a single-crystal QD buried in a single-crystal matrix.[22] We then use reported deformation potentials[23] to compute the spatial variations in band alignment.

Finally, to quantify the charge density distributions, the Schrödinger equation is solved within the single-particle effective mass approximation. Our model suggests that dislocation-induced strain relaxation and charging lead to significant local variations in the band alignment type and charge density distributions. Furthermore, misfit strain induces a transition from a nested (type I) to a staggered (type II) band alignment, consistent with the findings for planar structures in Refs. 7 and 8. The transition is reversed by dislocation-induced strain relaxation but restored by electrostatic charging at dislocation cores.

METHODS

In preparation for XSTM, GaSb/GaAs QD heterostructures[8] were thinned to ~150 μm using conventional mechanical polishing from the backside, as described in Ref. 24. The samples were cleaved to expose a (110) surface in an ultra-high vacuum (UHV) chamber with a base pressure of $<4 \times 10^{-11}$ Torr. STM was performed with commercially available Pt/Ir tips, which were cleaned *in situ* by electron bombardment. Since flat cleaves typically occur in the vicinity of the QD center, where the strain fields are highest, minimal surface height variations are expected in the XSTM image field of the view.[24] In addition, the GaAs (110) surface does not reconstruct; thus, surface electronic states are not expected.[25] Since we focus on the contributions of composition and strain to the band alignment, we make the simplifying assumption that the contrast in the constant-current STM images is due to variations in the $GaSb_xAs_{1-x}$ alloy composition, x, within GaSb-rich QDs.

Figure 1(a) shows a constant-current XSTM image in the vicinity of a GaSb/GaAs QD, with a 1.23 nm tip height color range displayed, with bright and dark regions corresponding to a GaSb-rich QD and GaAs matrix, respectively. The image was collected with a sample bias voltage of −2.6 V.[26] Similarly, XSTM images in Ref. 21 were collected at sample bias voltages in the range −2.5 to −4.0 V. These imaging conditions are relatively insensitive to electronic contrast, and similar band alignment predictions were obtained for both our image and the image from Ref. 21. For simplicity, we limit discussion to our image shown in Fig. 1(a). To differentiate GaSb-rich QDs and GaAs, we estimate a tip height criterion as follows. Bright regions with maximum tip heights ≥4.9 Å above the GaAs background were considered to be pure GaSb. Tip heights <4.9 Å above the GaAs background were considered $GaAs_{1-x}Sb_x$ alloys, where the composition value x was approximated by assuming a linear interpolation of the tip height values from GaAs and GaSb. It is interesting to note that variations in composition (x) are observed both within and outside of the QDs, as indicated by arrows in Fig. 1(a). Inhomogeneous composition is also observed outside of the QD, i.e., "exterior" Sb clusters, positioned at the corners of Fig. 1, similar to past reports on buried GaSb/GaAs nanostructures.[20,21,27] In Fig. 1(b), pixels with tip height up to 4.9 ± 0.5 Å above the GaAs background are displayed with bright to dark-gray scales attributed to increasing Sb fractions, x_{Sb}, from pure GaAs to pure GaSb (with local misfit ranging from 0 to 0.07).

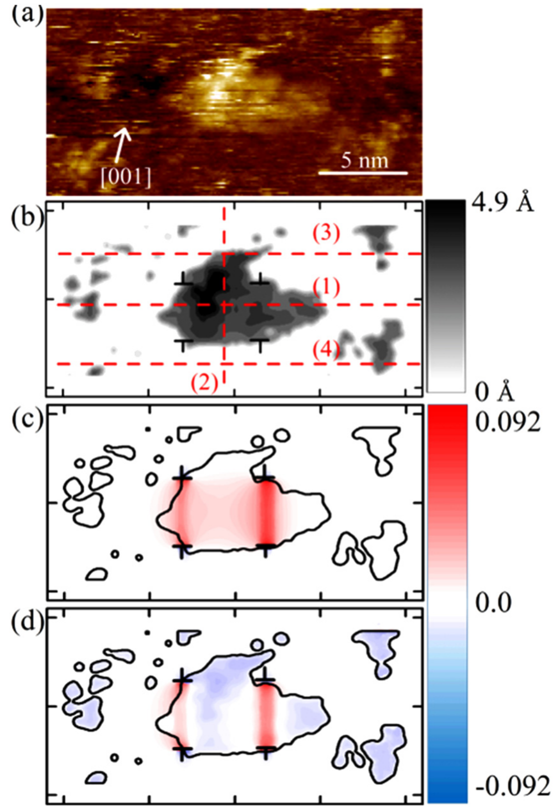

FIG. 1. (a) Cross-sectional scanning tunneling microscopy (XSTM) image, acquired in the vicinity of a GaSb/GaAs quantum dot (QD) using a constant tunneling current of 0.25 nA and a sample bias voltage of −2.6 V. The tip height color-scale range displayed is 1.23 nm, with bright and dark regions corresponding to GaSb-rich QD and the GaAs matrix, respectively. Pixels with tip height up to 4.9 ± 0.5 Å above the GaAs background in (a) are displayed in (b) with bright and dark-gray scales corresponding to increasing GaSb fractions, x_{Sb}. The removal of atomic planes in the GaSb-rich QDs is represented by the dislocation core symbols in (b), and the associated in-plane hydrostatic strain contours are shown in (c). The net in-plane hydrostatic strain contours, including both the misfit and dislocation-induced strain, are shown in (d). The red-dotted lines in (b) indicate paths along which band structure profiles will be presented.

To prepare the XSTM image data for input into the continuum model, the 2D distribution of Sb fractions was converted into a 3D composition profile using an axisymmetric rotation about the vertical axis of the QD, including the exterior clusters mentioned above. Using this 3D map of Sb fractions, we computed 3D profiles of the effective masses, permittivities, elastic constants, and deformation potentials, assuming linear interpolations of the values for the binary compounds GaAs and GaSb shown in Table I. The 3D composition profile was then interpolated onto a finite element mesh with periodic boundary conditions determined by the average QD separation in similarly grown samples, ~50 nm.[15] To consider the influence of

TABLE I. Continuum model parameters, with $m_0^* = 9.11 \times 10^{-31}$ kg.

Parameters	Symbol	GaSb	GaAs
Electron effective mass[39]	m_e/m_o^*	0.041	0.067
Hole effective mass[39]	m_h/m_o^*	0.40	0.47
Bandgap (eV)[40]	E_g	0.770	1.43
Valence band offset (eV)[18]	ΔE_v	−0.67−	
	a_c	−7.5	7.17
Deformation potential constants (eV)[41]	a_v	−0.8	−1.16
	b	−2.0	−2.0
	d	−4.7	−4.8
Lattice constant (Å)[42]	a_{lc}	6.0959	5.65325
Young's modulus (GPa)[43]	E	63.1	85.9

elastic misfit strain, we compute the 3D strain distribution using the isotropic linear elastic edge dislocation theory,[28] with edge dislocations spaced 5.5 nm apart at the top and bottom QD interfaces.[29] In this step, for simplicity, we have assumed the elastic constants to be spatially uniform—taking the average value of the GaAs and GaSb elastic constants—due to the lack of an analytical dislocation theory that can account for the full spatial variation; this simplification has a negligible effect on the results of the model. We note that this dislocation configuration is predicted to reduce the total energy of the system,[30] and it has been observed in capped GaSb/GaAs QDs,[31] InAs/GaAs QDs,[32] and InSb/GaAs QDs,[33] all with similar 7% misfit with respect to GaAs. The removal of atomic planes in the GaSb-rich QDs is represented by the dislocation loops in Fig. 1(b), with the associated in-plane hydrostatic strain contours shown in Fig. 1(c). The net in-plane hydrostatic strain contours, including both misfit and dislocation-induced strain, are shown in Fig. 1(d). We utilized the net strain 3D distribution to calculate rigid shifts in the VB and CB edges via the corresponding 3D profile of deformation potentials.

To consider the effects of dislocation charging, we treat Ga dangling bonds along the dislocation core as electron acceptors. We assume two dangling bonds per lattice site, each with occupancy, *sf*, such that the total line charge is $|sf(2q/a_{\mathrm{GaSb}})|$. We then compute the form of the electrostatic potential, $V(r)$, using Poisson's equation

$$\nabla^2 V(r) = -\frac{\rho(r)}{\varepsilon_0 \varepsilon_r(r)}, \tag{1}$$

where $\rho(r)$ is the spatially varying space charge, ε_0 is the permittivity of free space, and $\varepsilon_r(r)$ is a spatially varying permittivity assumed to follow the rule of mixtures. Since the total charge in the system must be zero,[34] a space charge density, ρ_{sc}, with equal magnitude and the opposite sign is induced, according to

$$\rho_{sc} = -\left|\frac{sf(2qL_{cores})}{a_{GaSb}V}\right|, \tag{2}$$

where L_{cores} is the added length of the two dislocation core centerlines and V is the total volume of the system. Ultimately, the space charge induces a 3D electrostatic potential, which is added as a rigid shift to the band offset.

Finally, to estimate the confinement induced by the spatially varying band edge profiles, we solve the steady-state Schrödinger equation in the effective mass approximation, equivalent to the **k·p** approach in a single band formulation. This simple approach is conveniently formulated using the finite element method and allows for an estimate of the energy levels and confinement of carriers[35] and, thus, the effective local band alignment type.

RESULTS AND DISCUSSION

The conduction band (CB) and valence band (VB) edge profiles calculated along the red-dotted lines, i.e., paths (1–4), in Fig. 1(b), are shown in Fig. 2 for the cases of (a) unstrained, (b) misfit strain, and (c–e) both misfit and dislocation strain with various degrees of dislocation charging: dangling bond site occupancy (d) $sf = 0.1$ and (e) $sf = 0.4$. Analogous band edge profiles for Smakman's QD image (Ref. 21) are presented in Fig. S1 in the supplementary material. To quantify type I vs type II alignment, we compare the local band energies along paths (1–4) in Fig. 1(b) to the GaAs matrix band energies at 1.43 eV (CB) and 0 eV (VB) reference levels. The relative positioning of these average values (as shown by the black dotted lines in Fig. 2) approximates the local alignment type. For the unstrained case in Fig. 2(a), a weak type I alignment is observed for paths across the QD center (paths 1 and 2), with minimal variations in band edges across the paths above and below the QD (paths 3 and 4). The CB offset (CBO) and VB offset (VBO), with values of 0.06 and 0.67 eV, are consistent with those predicted by model solid theory.[14] In Fig. 2(b), with the introduction of lattice misfit strain, a type II alignment is observed along paths 1 and 2, with minimal changes to the CBO and VBO along paths 3 and 4. However, the strained CBO of 0.2 eV is slightly higher than the measured values of 0.1 eV for (apparently) strained QDs.[36,37]

In Figs. 2(c)–2(e), the influences of dislocation strain and charging on GaSb/GaAs QD band edge profiles across paths 1–4 in Fig. 1(b) are considered. For path 1, the dislocation-induced strain fields reduce the energy of the GaSb CB edge in the vicinity of the dislocation cores, resulting in a local type I offset. For path 2, the GaSb CB edge is slightly higher in energy, leading to a lower average CBO of 0.1 eV, consistent with measured values for QDs[36,37] and QD rings.[38] For paths 3 and 4, in the vicinity of the dislocation cores, the CB edge is raised while the VB edge is lowered. Since the STM images were collected at a relatively "high" sample bias voltage of −2.6 V, the predicted variations in local VBO at the QD edges are not apparent in these images. Work is in progress to use sample bias voltages <−1 V to enhance the local-VBO-induced contrast variations in the vicinity of the QD edges, especially those features associated with strain and dislocation charging.

In Figs. 2(d) and 2(e), the influence of dislocation charging with dangling bond site occupancies $sf = 0.1$ and $sf = 0.4$, are shown. For $sf = 0.1$ in Fig. 2(d), the CB and VB profiles along paths 1–4 are very similar to the corresponding values for the calculations with misfit and dislocations strain in Fig. 2(c). With dislocation charging increased to $sf = 0.4$, both the CB and VB edges are reduced in the vicinity of the dislocation cores. Since this additional

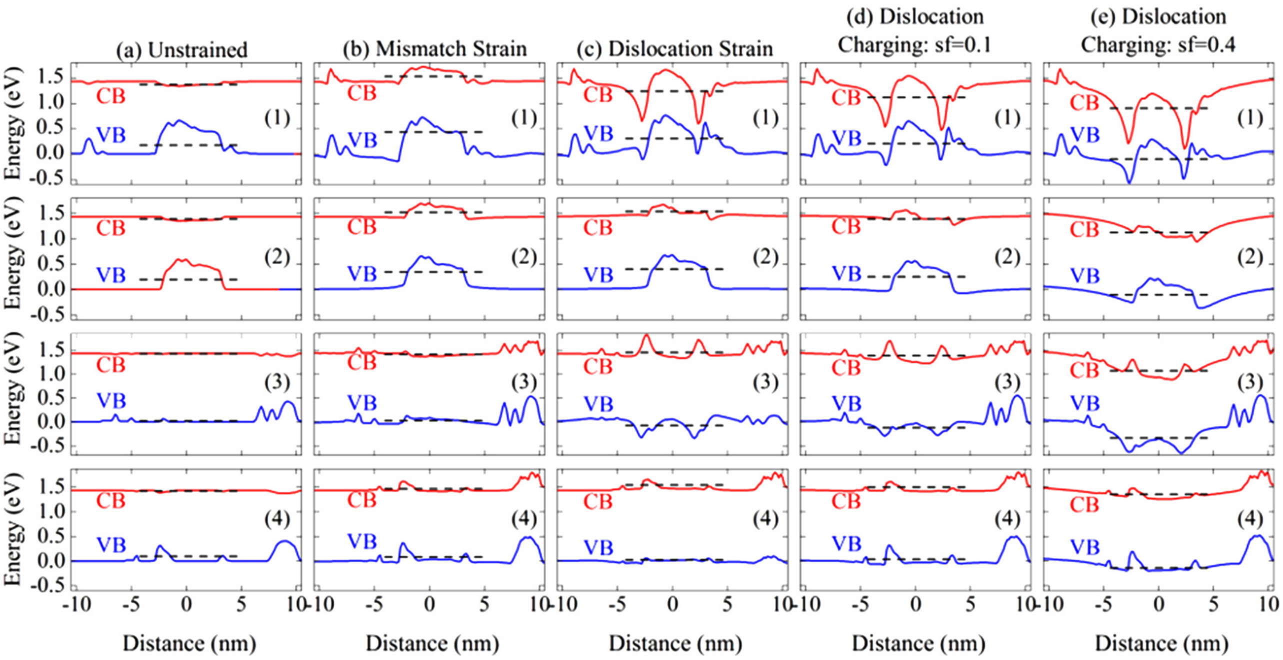

FIG. 2. Band profiles for the cases of (a) unstrained, (b) lattice mismatch strain, (c) dislocation strain, (d) dislocation charging of $sf = 0.1$, and (e) dislocation charging of $sf = 0.4$ across paths 1–4 from Fig. 1(b). The black dotted lines denote line-averaged band energies across the QD, with the GaAs matrix band energies at 1.43 eV (CB) and 0 eV (VB) as reference levels. For (a) the unstrained case, a weak type I alignment is observed for paths across the QD center (paths 1 and 2), with smaller band edge variations across paths above and below the QD (paths 3 and 4). In (b), with the introduction of misfit strain, the CB along paths 1 and 2 is raised, leading to type II band alignment; meanwhile, negligible changes to both CB and VB are observed along paths 3 and 4. In (c), with the inclusion of both misfit and dislocation strain, the band alignment is again type I across paths 1 and 2, with minimal change along paths 3 and 4. In (d), for $sf = 0.1$, the CB and VB values are similar to those in (c). Finally, in (e), for $sf = 0.4$, both CB and VB are lowered across paths 1–4, resulting in type II band alignments.

electrostatic potential equally displaces the CB and VB edges, the classification of band alignment type in 1D is not obvious. In addition, band bending due to the charged dislocation cores induces complex potential profiles that may increase or decrease the spatial overlap of electron or hole states based on the spatially varying effective mass. For the higher site occupancy, $sf = 0.4$, the average band alignment is apparently type II. To confirm this observation, we consider 3D solutions to the Schrödinger equation.

For an unstrained GaSb/GaAs QD, the normalized ground state hole and electron charge densities are shown in Fig. 3(a). The

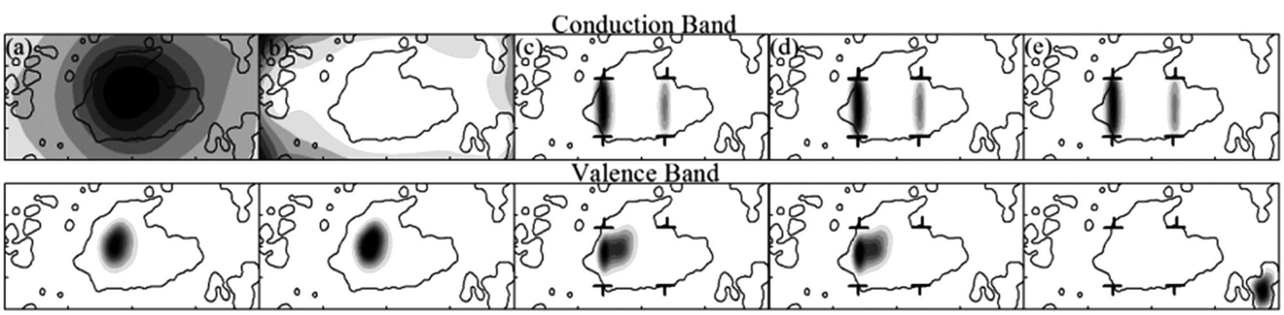

FIG. 3. Effective mass computations of normalized probability densities for the ground electron and hole states, with darker shading representing higher densities. The top row shows conduction band solutions, while the bottom row shows valence band solutions for (a) unstrained QDs, (b) with misfit strain, (c) misfit and dislocation strain, (d) with misfit and dislocation strain plus dislocation charging with dangling bond site occupancy $sf = 0.1$, and (e) with misfit and dislocation strain plus dislocation charging with dangling bond site occupancy $sf = 0.4$. Consistent with the band alignment shown in Fig. 2, spatial separation of the conduction band and valence band charge densities characteristic of type II band alignment is shown in (b) and (e).

ground state hole and electron charge densities, calculated with the inclusion of (b) misfit strain, (c) misfit and dislocation strain, as well as misfit and dislocation strain plus dislocation charging with dangling bond site occupancy (d) $sf = 0.1$ and (e) $sf = 0.4$, are also included in Fig. 3. For the unstrained QD shown in Fig. 3(a), the ground state charge densities are highest within the center of the QD, revealing the spatial coexistence of electron and hole states expected for a type I offset. In Fig. 3(b), the inclusion of misfit strain induces an increase in hole density within the GaSb-rich QD and an increase in electron density within the GaAs matrix, leading to the type II offset described above. As shown in Fig. 3(c), with the addition of dislocation strain, both electron and hole charge densities are confined at the GaSb-rich QD/GaAs interface, specifically between the dislocation cores, consistent with a local type I band alignment. Similar effects are observed with the addition of minimal dislocation charging, $sf = 0.1$, as shown in Fig. 3(d). Finally, with a further increase in dislocation charging to $sf = 0.4$, the ground state hole density shifts to an exterior GaSb cluster outside the QD, while the ground state electron density remains confined between the dislocation cores, leading to the spatial separation of electron and hole states expected for a type II offset.

CONCLUSION

In summary, we have investigated the influence of strain and dislocations on band alignments in GaSb/GaAs QD systems. We used a combined experimental and computational approach that permits us to separately consider the contributions of strain and dislocations. Using composition profiles from XSTM images of GaSb/GaAs QDs as input into a continuum model, we examine the effects of misfit strain, dislocation strain, and dislocation charging on CB and VB edge profiles. For an unstrained GaSb/GaAs QD, a weak type I band alignment is predicted. With the addition of misfit strain, a transition to a type II band alignment is observed. However, the inclusion of additional effects such as dislocation strain and/or dislocation charging leads to local restorations of type I and/or type II alignment. Therefore, variations in QD morphologies and dislocation positions/orientations may be used to tune the coexistence of local type I and type II band alignments. Further work is in progress to explore correlations between local QD morphologies, dislocation configurations, and local band alignments in buried QD ensembles.

SUPPLEMENTARY MATERIAL

See the supplementary material for band edge profiles computed using an XSTM image of the GaSb/GaAs QD structure from Ref. 21.

ACKNOWLEDGMENTS

We gratefully acknowledge the support of the U.S. Department of Energy, Office of Science, Office of Basic Energy Sciences, under Grant No. DE-FG02-06EF46339. The work was also supported, in part, by the National Science Foundation through the Graduate Research Fellowship Program (No. DGE-1256260) and Grant No. ECCS-1610362.

AUTHOR DECLARATIONS

Conflict of Interest

The authors have no conflicts to disclose.

DATA AVAILABILITY

The data that support the findings of this study are available from the corresponding author upon reasonable request.

REFERENCES

[1] M. Geller, C. Kapteyn, L. Müller-Kirsch, R. Heitz, and D. Bimberg, "450 MeV hole localization in GaSb/GaAs quantum dots," Appl. Phys. Lett. **82**, 2706 (2003).

[2] M. Hayne, R. J. Young, E. P. Smakman, T. Nowozin, P. Hodgson, J. K. Garleff, P. Rambabu, P. M. Koenraad, A. Marent, L. Bonato, A. Schliwa, and D. Bimberg, "The structural, electronic and optical properties of GaSb/GaAs nanostructures for charge-based memory," J. Phys. D: Appl. Phys. **46**, 264001 (2013).

[3] R. B. Laghumavarapu, A. Moscho, A. Khoshakhlagh, M. El-Emawy, L. F. Lester, and D. L. Huffaker, "GaSb/GaAs type II quantum dot solar cells for enhanced infrared spectral response," Appl. Phys. Lett. **90**, 173125 (2007).

[4] Y. Shoji, R. Tamaki, and Y. Okada, "Multi-stacked GaSb/GaAs type-II quantum nanostructures for application to intermediate band solar cells," AIP Adv. **7**, 5305 (2017).

[5] P. J. Carrington, A. S. Mahajumi, M. C. Wagener, J. R. Botha, Q. Zhuang, and A. Krier, "Type II GaSb/GaAs quantum dot/ring stacks with extended photoresponse for efficient solar cells," Phys. B: Condens. Matter **407**, 1493 (2012).

[6] J.-B. Wang, S. R. Johnson, S. A. Chaparro, D. Ding, Y. Cao, Y. G. Sadofyev, Y.-H. Zhang, J. A. Gupta, and C. Z. Guo, "Band edge alignment of pseudomorphic $GaAs_{1-y}Sb_y$ on GaAs," Phys. Rev. B **70**, 195339 (2004).

[7] C. Jones and E. Kioupakis, "Effect of strain on band alignment of GaAsSb/GaAs quantum wells," J. Appl. Phys. **122**, 045703 (2017).

[8] C. Greenhill, A. S. Chang, E. S. Zech, S. Clark, G. Balakrishnan, and R. S. Goldman, "Influence of quantum dot morphology on the optical properties of GaSb/GaAs multilayers," Appl. Phys. Lett. **116**, 252107 (2020).

[9] M. Tytus, J. Krasnyj, W. Jacak, A. Chuchmała, W. Donderowicz, and L. Jacak, "Differences between photoluminescence spectra of type-I and type-II quantum dots," J. Phys.: Conf. Ser. **104**, 12011 (2008).

[10] J. Tatebayashi, A. Khoshakhlagh, S. H. Huang, L. R. Dawson, G. Balakrishnan, and D. L. Huffaker, "Formation and optical characteristics of strain-relieved and densely stacked GaSb/GaAs quantum dots," Appl. Phys. Lett. **89**, 203116 (2006).

[11] C.-C. Tseng, S.-C. Mai, W.-H. Lin, S.-Y. Wu, B. -Y. Yu, S. -H. Chen, S.-Y. Lin, J.-J. Shyue, and M.-C. Wu, "Influence of as on the morphologies and optical characteristics of GaSb/GaAs quantum dots," IEEE J. Quantum Electron. **47**, 335 (2011).

[12] N. N. Ledentsov, J. Böhrer, M. Beer, F. Heinrichsdorff, M. Grundmann, D. Bimberg, S. V. Ivanov, B. Ya. Meltser, S. V. Shaposhnikov, I. N. Yassievich, N. N. Faleev, P. S. Kop'Ev, and Zh. I. Alferov, "Radiative states in type-II GaSb/GaAs quantum wells," Phys. Rev. B **52**, 14058 (1995).

[13] E. S. Zech, A. S. Chang, A. J. Martin, J. C. Canniff, Y. H. Lin, J. M. Millunchick, and R. S. Goldman, "Influence of surface termination on GaSb/GaAs quantum dot structure and band offsets," Appl. Phys. Lett. **103**, 082107 (2013).

[14] P. Sitarek, H. P. Hsu, Y. S. Huang, J. M. Lin, H. H. Lin, and K. K. Tiong, "Optical studies of type-I $GaAs_{1-x}Sb_x$/GaAs multiple quantum well structures," J. Appl. Phys. **105**, 123523 (2009).

[15] S. V. Morozov, D. I. Kryzhkov, A. N. Yablonsky, A. V. Antonov, D. I. Kuritsin, D. M. Gaponova, Yu. G. Sadofyev, N. Samal, V. I. Gavrilenko, and Z. F. Krasilnik, "Type II-type I conversion of GaAs/GaAsSb heterostructure energy spectrum under optical pumping," J. Appl. Phys. **113**, 163107 (2013).

[16] M. Dinu, J. E. Cunningham, F. Quochi, and J. Shah, "Optical properties of strained antimonide-based heterostructures," J. Appl. Phys. **94**, 1506 (2003).

[17]M. Jo, M. Sato, S. Miyamura, H. Sasakura, H. Kumano, and I. Suemune, "Origin of the blueshift of photoluminescence in a type-II heterostructure," Nanoscale Res. Lett. **7**, 654 (2012).
[18]C. G. Van de Walle, "Band lineups and deformation potentials in the model-solid theory," Phys. Rev. B. **39**, 1871 (1989).
[19]G. Balakrishnan, J. Tatebayashi, A. Khoshakhlagh, S. H. Huang, A. Jallipalli, L. R. Dawson, and D. L. Huffaker, "III/V ratio based selectivity between strained Stranski-Krastanov and strain-free GaSb quantum dots on GaAs," Appl. Phys. Lett. **89**, 161104 (2006).
[20]R. Timm, A. Lenz, H. Eisele, L. Ivanova, M. Dähne, G. Balakrishnan, D. L. Huffaker, I. Farrer, and D. A. Ritchie, "Quantum ring formation and antimony segregation in GaSb/GaAs nanostructures," J. Vac. Sci. Technol. B **26**, 1492 (2008).
[21]E. P. Smakman, J. K. Garleff, R. J. Young, M. Hayne, P. Rambabu, and P. M. Koenraad, "GaSb/GaAs quantum dot formation and demolition studied with cross-sectional scanning tunneling microscopy," Appl. Phys. Lett. **100**, 142116 (2012).
[22]V. V. Chaldyshev, N. A. Bert, A. L. Kolesnikova, and A. E. Romanov, "Stress relaxation scenario for buried quantum dots," Phys. Rev. B **79**, 233304 (2009).
[23]S.-H. Wei and A. Zunger, "Predicted band-gap pressure coefficients of all diamond and zinc-blende semiconductors: Chemical trends," Phys. Rev. B **60**, 5404 (1999).
[24]B. Lita, R. S. Goldman, J. D. Phillips, and P. K. Bhattacharya, "Nanometer-scale studies of vertical organization and evolution of stacked self-assembled InAs/GaAs quantum dots," Appl. Phys. Lett. **74**, 2824 (1999).
[25]R. M. Feenstra, "Tunneling spectroscopy of the (110) surface of direct-gap III-V semiconductors," Phys. Rev. B **50**, 4561 (1994).
[26]R. Timm, R. M. Feenstra, H. Eisele, A. Lenz, L. Ivanova, E. Lenz, and M. Dähne, "Contrast mechanisms in cross-sectional scanning tunneling microscopy of GaSb/GaAs type-II nanostructures," J. Appl. Phys. **105**, 093718 (2009).
[27]E. P. Smakman, M. DeJarld, M. Luengo-Kovac, A. J. Martin, V. Sih, P. M. Koenraad, and J. Millunchick, "Height stabilization of GaSb/GaAs quantum dots by Al-rich capping," APL Mater. **2**, 096111 (2014).
[28]J. P. Hirth and J. Lothe, *Theory of Dislocations*, 2nd ed (John Wiley & Sons, 1982).
[29]S. Huang, G. Balakrishnan, and D. L. Huffaker, "Interfacial misfit array formation for GaSb growth on GaAs," J. Appl. Phys. **105**, 103104 (2009).
[30]H. T. Johnson and L. B. Freund, "Mechanics of coherent and dislocated island morphologies in strained epitaxial material systems," J. Appl. Phys. **81**, 6081 (1997).
[31]N. Fernández-Delgado, M. Herrera, M. F. Chisholm, M. A. Kamarudin, Q. D. Zhuang, M. Hayne, and S. I. Molina, "Atomic-column scanning transmission electron microscopy analysis of misfit dislocations in GaSb/GaAs quantum dots," J. Mater. Sci. **51**, 7691 (2016).
[32]L. Dai, S. P. Bremner, S. Tan, S. Wang, G. Zhang, and Z. Liu, "Suppression of dislocations by Sb spray in the vicinity of InAs/GaAs quantum dots," Nanoscale Res. Lett. **9**, 278 (2014).
[33]S. Shusterman, A. Raizman, A. Sher, A. Schwarzman, O. Azriel, A. Boag, Y. Rosenwaks, P. L. Galindo, and Y. Paltiel, "Two-dimensional imaging of III-V quantum dots confinement potential," Europhys. Lett. **88**, 66003 (2009).
[34]W. H. Hayt, *Engineering Electromagnetics*, 3d ed (McGraw-Hill, 1974).
[35]H. T. Johnson, L. B. Freund, C. D. Akyüz, and A. Zaslavsky, "Finite element analysis of strain effects on electronic and transport properties in quantum dots and wires," J. Appl. Phys. **84**, 3714 (1998).
[36]M. E. Rubin, H. R. Blank, M. A. Chin, H. Kroemer, and V. Narayanamurti, "Local conduction band offset of GaSb self-assembled quantum dots on GaAs," Appl. Phys. Lett. **70**, 1590 (1997).
[37]F. Hatami, N. N. Ledentsov, M. Grundmann, J. Böhrer, F. Heinrichsdorff, M. Beer, D. Bimberg, S. S. Ruvimov, P. Werner, U. Gösele, J. Heydenreich, U. Richter, S. V. Ivanov, B. Ya. Meltser, P. S. Kop'Ev, and Zh. I. Alferov, "Radiative recombination in type-II GaSb/GaAs quantum dots," Appl. Phys. Lett. **67**, 656 (1995).
[38]R. Timm, H. Eisele, A. Lenz, L. Ivanova, V. Vossebürger, T. Warming, D. Bimberg, I. Farrer, D. A. Ritchie, and M. Dähne, "Confined states of individual type-II GaSb/GaAs quantum rings studied by cross-sectional scanning tunneling spectroscopy," Nano Lett. **10**, 3972 (2010).
[39]F. J. Blatt, *Modern Physics* (McGraw-Hill Book Company, Inc., 1992).
[40]C. Kittel, *Introduction to Solid State Physics, 8th Ed.*, 6th ed (John Wiley & Sons, 1986).
[41]E. T. Yu, J. O. McCaldin, and T. C. McGill, "Band offsets in semiconductor heterojunctions," Solid State Phys. **46**, 1 (1992).
[42]I. Vurgaftman, J. R. Meyer, and L. R. Ram-Mohan, "Band parameters for III-V compound semiconductors and their alloys," J. Appl. Phys. **89**, 5815 (2001).
[43]S. Adachi, *Physical Properties of III-V Semiconductor Compounds: InP, InAs, GaAs, GaP, InGaAs, and InGaAsP* (John Wiley & Sons, 1992).